Epsilon Aurigae: Deriving a Baade-Wesselink Distance

by

Christine K. Wilson

A THESIS SUBMITTED IN PARTIAL FULFILMENT OF
THE REQUIREMENTS FOR THE DEGREE OF

BACHELOR OF SCIENCE

in

Honours Astrophysics

(Department of Astronomy and Physics, Dr. Philip D. Bennett supervising faculty)

.....

.....

.....

.....

.....

SAINT MARY'S UNIVERSITY

May 11, 2013

Abstract

Epsilon Aurigae: Deriving a Baade-Wesselink Distance

by Christine K. Wilson

Epsilon Aurigae is a third magnitude, long-period binary that eclipses every 27.1 years and has been continuously observed for more than 160 years. The observed spectrum is that of an apparently normal F supergiant. The duration of the eclipse and the amplitude of the derived radial velocity orbit imply the presence of a massive companion; however, this eclipsing companion is dark.

In addition to the strange nature of this binary, previous distance estimates to this system have provided inaccurate results. The HIPPARCOS satellite measured a parallax of 1.53 ± 1.29 mas, which gives a nominal distance of $0.35 - 4.2$ pc (van Leeuwen, 2007). Without an understanding of the distance to the system, absolute parameters, such as the mass and evolutionary state, of the system cannot be determined.

This thesis project focuses on a spectroscopic and photometric analysis of the F0 supergiant in this enigmatic, long period eclipsing binary. Archival U, B, V, R, I, J, and H photometric data compiled by Hopkins (2012), and radial velocity data from Stefanik et al. (2010), Chadima et al. (2010), and Eaton (2013) were used to analyze the irregular variability of the supergiant. Using a variation of the Baade-Wesselink method, commonly used for Cepheid distance determination, an estimate of the distance to this system can be derived. A more complete data set, selected for simultaneous optical and infrared photometric and radial velocity coverage, is necessary to provide accurate results with this proposed method. Suggestions for future observations and analysis are discussed.

Submitted on May 11, 2013

Contents

List of Figures

Chapter 1

Introduction

1.1 Epsilon Aurigae, a Mysterious System

Epsilon Aurigae (ε Aur) is a third magnitude, long-period binary that eclipses every 27.1 years. This system consists of an F supergiant and an unseen companion. The geometric, flat-bottomed eclipse lasts for approximately two years, during which the dark companion occults nearly half of the primary star's disk. The duration and extent of the eclipse, as well as the amplitude of the derived radial velocity orbit, imply the presence of a massive companion; however, this eclipsing companion has not been directly observed. No light is seen from this object in the optical spectrum, and few emission lines have been detected in the spectrum during eclipse. As such, no secondary eclipse has been detected for this system.

The first recorded eclipse of ε Aur was by Fritsch in 1821, and has subsequently been continuously observed. Since then, the system has undergone seven long-awaited primary eclipses, each shedding further light on the nature of this astronomical anomaly through decades of advancements in technology.

Initially, Kuiper et al. (1937) proposed the dark companion must be a large, extended, partially transparent star. This scenario was replaced by the proposed disk model, presented by Huang (1965). The companion is now believed to be a B star,

embedded within an opaque disk, which is seen edge-on. During the most recent eclipse in 2009-2011, ε Aur was imaged by the Center for High Angular Resolution Astronomy (CHARA) array of telescopes on Mt. Wilson, CA, in the visible and near-infrared wavelengths (Kloppenborg et al., 2010). This was the first image produced of a binary star system in eclipse, and provided direct confirmation of the Huang (1965) model (figure 1.1).

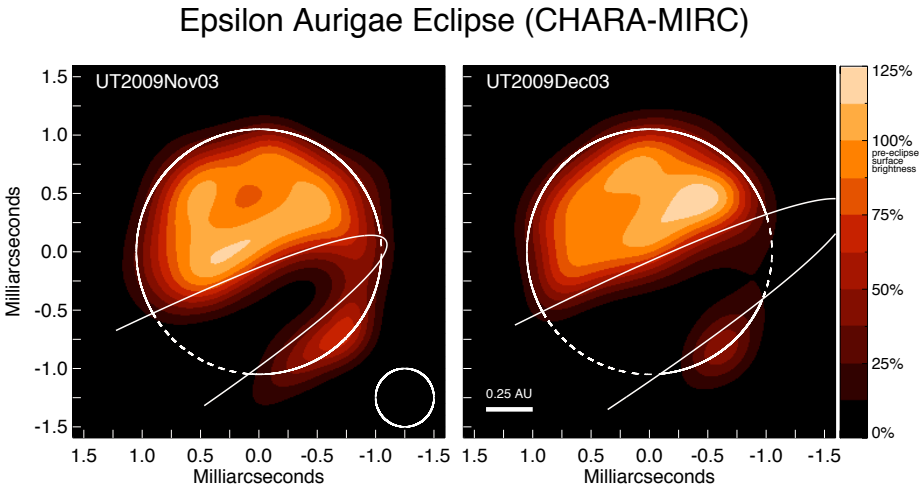

Figure 1.1: Image of ingress of eclipse of ε Aurigae taken with CHARA. Figure produced by John D. Monnier of the University of Michigan (Kloppenborg et al., 2010).

While the primary F supergiant is easily visible to the naked eye, little is known about the system because of the unseen nature of the companion. The observed spectrum is that of an apparently normal F supergiant. This star undergoes semi-regular pulsations in magnitude with a period of approximately 67 days. The recent PHOEBE and FOTEL orbital solutions derived by Stefanik et al. (2010) and Chadima et al. (2010), produced through spectroscopic radial velocity determinations, lead to agreeable results. The orbital period of $P \sim 9890.5$ days, and an eccentricity

of $e = 0.253 \pm 0.014$ have been determined. The disk temperature, from studies of photometry in the infrared by Taranova & Shenavrin (2001), has been inferred between $400 - 1000$ K. The derived temperature of the disk has been proposed to arise from either heating by the supergiant or kinetic heating within the disk. The disk is also measured to be inclined to our line of sight, by a value of $\sim 2^o$. The orbit of the system is shown in figure 1.2.

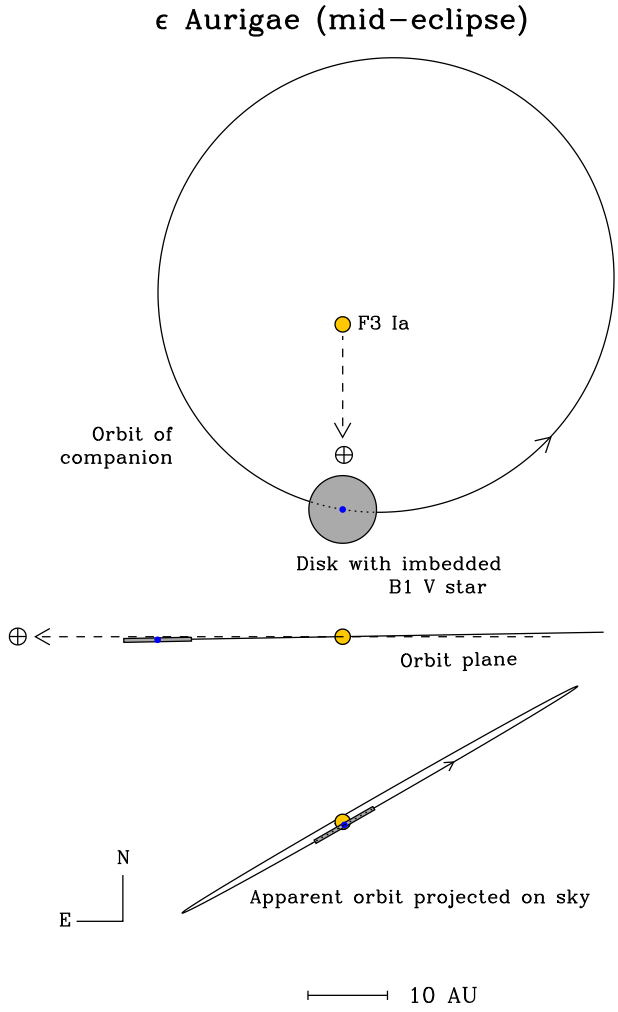

Figure 1.2: Orbit of ε Aurigae pictured from above, in the orbital plane, and the projection on sky. Bennett (2013), private communication.

Two scenarios regarding the nature of the system have been considered, based on the distance to, and thus the mass of, the binary. If the system is a near, low-mass binary, the F star could be a highly evolved post-asymptotic giant branch (post-AGB) star. The orbital parameters for this situation would support mass transfer between the primary and the companion. Another possibility, if the system is distant, is that the pair is a high-mass binary. At large distances, the separation between the two stars would be large, and imply no mass transfer has occurred. This would indicate the disk enveloping the unseen star is of protoplanetary origin.

1.2 Previous Distance Studies

The absolute parameters of this system are all dependent on our knowledge of its distance, which is currently poorly known. Stothers (1971) estimated the distance to ε Aur by its potential association as a member of the Aur OB1 cluster, which would place the system around 1340 pc. The parallax from the revised HIPPARCOS reduction of van Leeuwen (2007) gave 1.53 ± 1.29 mas, implying an uncertain distance of $0.35 - 4.2$ kpc; The star is just too far away for an accurate parallax distance determination.

Given the primary's spectral classification of an F0I star, certain limits can be placed on the minimum distance by theoretical absolute magnitudes. With a visual magnitude $m_V = 3$mag, the absolute magnitude of ε Aur could be between $-8.0 < M_V < -6.6$ mag, depending on the evolutionary state of the star. Stencel (2012) states that a yellow supergiant with this magnitude would place the star at a distance

of at least 740 pc.

Recently, Guinan et al. (2012) estimated the distance to the system by a study of interstellar absorption and reddening. Analyzing these quantities for nearby stars along the line of sight to ε Aur, they derived a distance of 1.5 ± 0.5 kpc. These results would designate ε Aur as a distant, high-mass, young binary system.

1.3 Baade-Wesselink Distance Method

Here we focus on the nature of the F supergiant by determining the distance to the system. The Baade-Wesselink distance method was developed to capitalize on the regular pulsations of Cepheids. A star's luminosity is dependent on its surface area and brightness; therefore, in knowing the amount by which a Cepheid's surface area is changing, and the brightness, at its minimum and maximum, a distance may be derived. The ratio by which the radius changes between its brightest and dimmest state can be determined by its change in magnitude, while the difference in these radii can be determined by radial velocity measurements (Turner, 2012).

By analyzing the quasi-periodic pulsations of the star in both the available photometry and radial velocity data for the star, details can be inferred about the size of the star. Broadband photometric data obtained prior to, and during, the latest 2009-11 eclipse were used to derive effective temperatures and angular diameters at each epoch from Lejeune et al. (1997) atmospheres to the spectral energy distribution. By comparing the changes in angular diameter with the changes in radial velocity, a Baade-Wesselink distance to the system can be derived.

Chapter 2

Observations and Data Reduction

2.1 Photometric Data

The photometric data used in the analysis were obtained from Hopkins (2012), who spearheaded the ground-based photometric observation campaign of ε Aur. Archival photometry in the U, B, V, R, I, J, and H bands of the F-star outside of eclipse, from January 1985 through April 2009, from over 20 observers worldwide was examined. The limited Taranova & Shenavrin (2001) infrared photometry were also included to supplement the photometry for this analysis.

Additional photometric data was analyzed through the 1982-84 and 2009-11 eclipses. Additional interest in the system during eclipse, especially from the influence of the Citizen Science effort by Stencel (2008) to involve amateur astronomers, provided significant coverage of photometry in eclipse. These data, compiled by Hopkins (2012) were used for additional analyses.

2.2 Radial Velocity Data

The radial velocity dataset was compiled from Stefanik et al. (2010) and Chadima et al. (2010). For the present analysis, the PHOEBE and FOTEL orbital solutions of Chadima et al. (2010) were averaged to obtain a mean solution used to remove the

binary motion. Any remaining radial velocity variability was assumed to be intrinsic to the F star. Recently, ε Aur radial velocity measurements of Eaton (2013) during the 2009-11 eclipse were also included. The Eaton dataset were obtained by the 2m Tennessee State University automated spectroscopic telescope, which obtained spectra of ε Aur during nearly every available clear night from mid-2008 through mid-2011. These radial velocity datasets were merged and smoothly interpolated onto a uniform time grid with the photometry, as will be discussed in §3.

2.3 Cleaning Method

With many observers, using a variety of equipment, in various locations and conditions, there was innate error in the photometric and radial velocity datasets. The continuity and quality of these data were essential for this analysis; therefore, processing these datasets to remove and correct inconsistent data (henceforth referred to as 'cleaning') was essential. Any observers who contributed :

1. small datasets or datasets of limited duration

2. datasets with significantly discrepant means, or

3. datasets with large standard deviations

were rejected. With the remaining datasets, data points beyond three standard deviations of the observers mean were eliminated and the dataset means were corrected to the mean value listed on the SIMBAD database. After this cleaning procedure, only the long-term observational time series of Jeffrey L. Hopkins at Hopkins Phoenix Ob-

servatory, Louis Boyd at Fairborn Observatory, and Brian E. McCandless at Grand View Observatory were retained for this analysis. Figure 2.1 shows the difference between the original data and the cleaned data for the B-band.

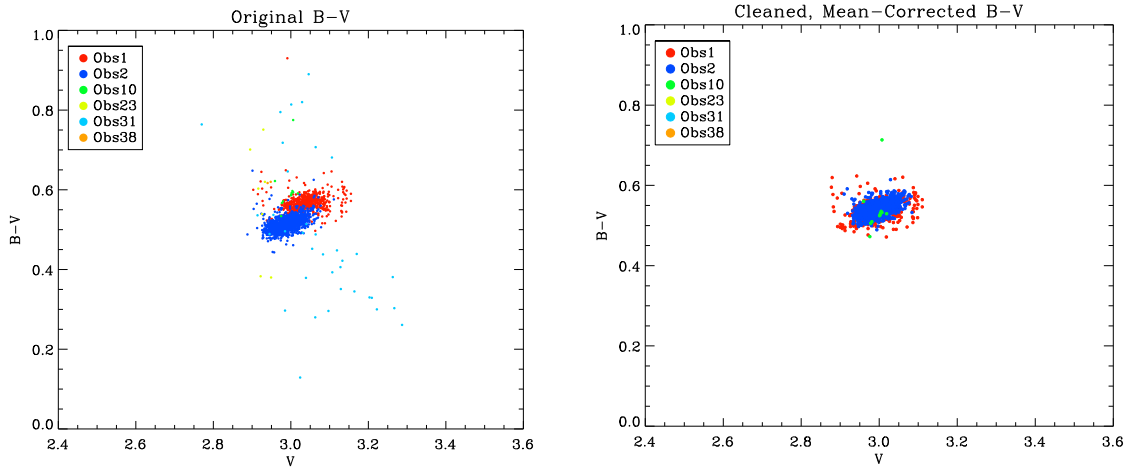

(a) Original Data

(b) Data after cleaning

Figure 2.1: Sample of the cleaning procedure applied to B band data, as compared to V. Various colours indicate different observers.

2.4 Reconstruction of Synthetic J-band Photometry

With the cleaned photometric data series, zero-point offsets were applied to bring the individual observer means into agreement with the mean values of UBV and JP11 photometry from the SIMBAD database. Of the U, B, V, R, I, J, and H photometric data considered, only the U, B, and V data were adequately sampled to permit interpolation to a regular time grid.

To properly bracket the peak of the stellar spectral energy distribution (SED) and properly constrain the stellar flux model fits, infrared (IR) data was necessary. There

were limited amounts of infrared data available for the R, I, J, H, or K bands. The intent was to use mean colour-colour relations to derive a suitable IR time sequence from the interpolated U, B, and V data. From the limited amounts of archival R, I, J, and H data available, the J band provided the most correlation between the V, U-B and B-V. A variety of colour-colour relations were sought, and results will be discussed for the following scenarios:

1. J derived from U-B, B-V, and V-J colours (§2.4.1).

2. J derived from relationship with V magnitudes magnitudes of photometry from the middle of the 2009-11 eclipse (§2.4.2).

3. J derived from relationship between ΔJ and ΔV magnitudes of photometry from the middle of the 1982-84 eclipse (§2.4.3).

Unfortunately, in all cases, little correlation was found to provide trustworthy J magnitudes. For these reasons, the derived distances, as will be discussed in §5, are not definitive results.

2.4.1 J derived from U-B and V-J colours

A first attempt to recreate J photometry was pursued using the U-B, B-V and V-J colours. The method used to develop a mean colour-colour relation was by a linear least-squares fit in three dimensions of the form

$$V - J = \alpha + \beta(U - B) + \gamma(B - V), \tag{2.1}$$

where α, β, and γ are the parameters for the fit between the U-B, B-V and V-J values. Standard least-squares regression fits treat the independent and dependent variables differently, with all the statistical error assumed to be present in the dependent variable. In this situation, fitting $y = f(x)$ can yield significantly different solutions than fitting $x = f(y)$. This assumption of classical least-squares fitting does not hold for fits of colour-colour relations between photometric data in which both datasets posses comparable noise. Isobe et al. (1990) addressed this problem by developing a symmetric form of least-squares fitting: the bisector lines of the standard $y - x$ and $x - y$ regression lines. The Isobe et al. (1990) fits are symmetric with respect to the variables, the same fit is obtained assuming either variable is the independent one.

For the three-colour fit needed here, we used a generalization of the Isobe et al. (1990) method to three (or more) variables, as described in Bennett & Wilson (2013). The source code developed for this fitting procedure is provided in appendix A. For this situation, the variation in all colours vary from the intrinsic pulsations of the star, and thus the scatter in the data should be treated symmetrically in all variables to provide an accurate fit. Assuming that J always varied in a similar manner with U, B, and V during stellar pulsations, a mean relation was found, as pictured in figure 2.2. For the available data, this relation was:

$$V - J = 0.854 - 0.273(B - V) - 0.533(U - B). \tag{2.2}$$

However, upon examination the U data presented inconsistencies and was not in agreement with archival UBV and JP11 photometry from the SIMBAD database.

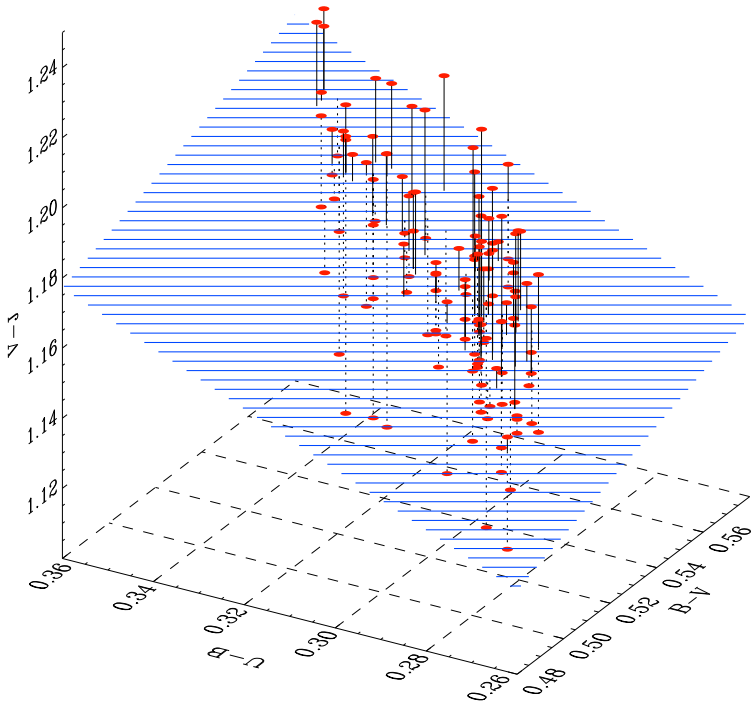

Figure 2.2: Relationship between U-B, B-V and B-J produced through a 3-D generalization of the Isobe least-squares bisection regression.

The U band presents particular problems for amateur astronomers because the short wavelength edge of the band is defined by the atmosphere cutoff, and this has not been calibrated for most amateur photometry. It was thought a more accurate relationship would be obtained by using only the B-V and V-J colours. Again, the Isobe et al. (1990) method, which only handles two variables, was used to derive a mean relation for V-J and B-V; however, these values were found to be largely uncorrelated. The resulting linear fit explained little of the variance in the J band data.

2.4.2 J derived from V magnitudes during 2009-11 eclipse

With more IR photometry available during the eclipse, the colour-colour relationships for the photometry were also analyzed from the 2009-11 eclipse data from Hopkins

(2012). Since the eclipse is nearly grey, where all passbands are affected equally by the eclipse, there is little effect on the colour-colour relations. Therefore, the eclipse colour-colour relationships derived should be applicable to the out-of-eclipse data.

Additional sampling of data in eclipse was available, however, the colours were found to be largely uncorrelated as well. As seen in figure 2.3, the J and H data vary minimally as compared to B and V data, and do not appear to show the same instrinsic variation as seen in B and V. The implications of these results are discussed in §6. The correlations between V, J and H photometry were improved, 2.4, however these are still not significantly correlated.

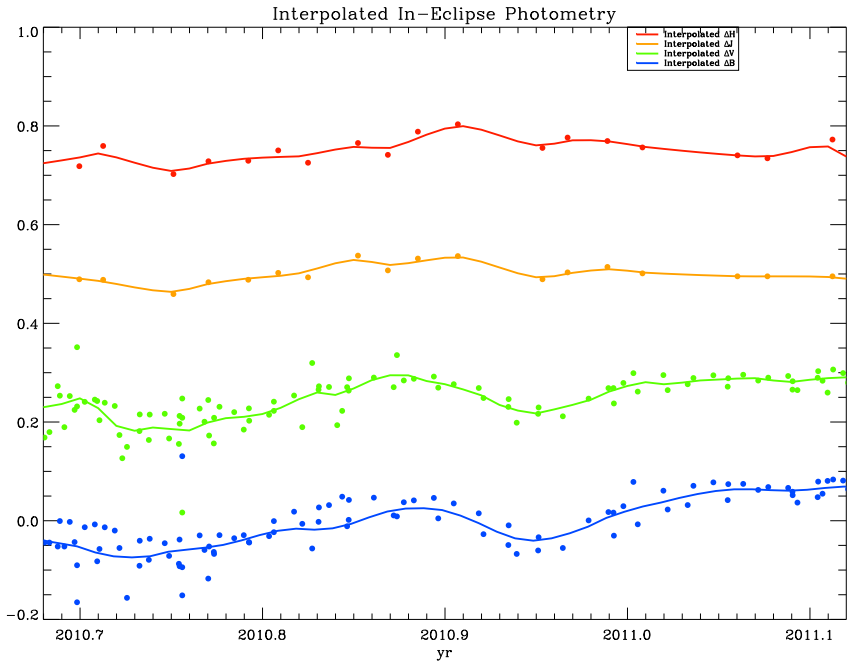

Figure 2.3: Interpolated in eclipse photometry in B, V, J, and H bands. Variations from the mean magnitudes are plotted, with arbitrary offsets for improved visualization.

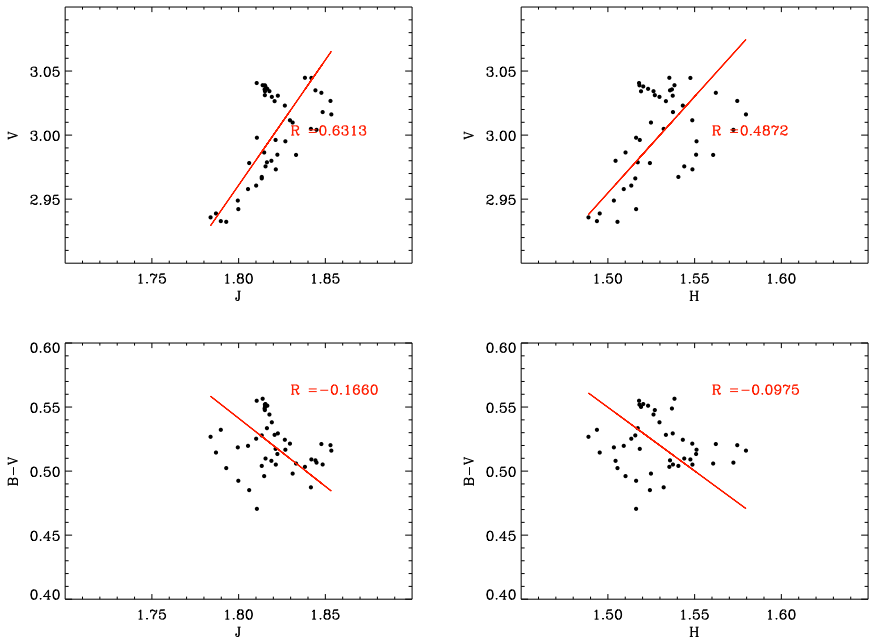

Figure 2.4: Correlations (R) between B, V, J and H photometry in eclipse totality.

The relationships used to reconstruct the J and H band photometry were

$$J = 0.512V + 0.285 \tag{2.3}$$

and

$$H = 0.664V - 0.463, \tag{2.4}$$

as stronger relationships existed between the V magnitudes and the available J and H photometry in eclipse.

2.4.3 J derived from V magnitudes during 1982-84 eclipse

A final attempt was made to produce a reliable J dataset from data available during the 1982-84 eclipse from Taranova & Shenavrin (2001). Approximately 20 data

points from U, B, V, J, H and K from mid-eclipse were analyzed. Although there was significant scatter, the J and K magnitudes vary opposite to that of the optical magnitudes. The cleanest fit found was for the differences in J, ΔJ, as compared to the differences in V, ΔV, from their respective means. By necessity, this fit must go through $(0.0, 0.0)$, so all that's being fit is the slope. For ΔJ versus ΔV, the derived relationship was

$$\Delta J = -1.001 \Delta V \tag{2.5}$$

This relation was corrected for the Hopkins out-of-eclipse B and V data to generate synthetic J band data.

Chapter 3

Interpolation

A few methods of interpolation were tested to create a continuous time series of photometric and radial velocity data. A method of smoothly interpolating non-uniformly spaced, sporadic data, sometimes with multiple concurrent observations, and large seasonal gaps, was needed.

3.1 Weighting Function Interpolation

Each of the U, B, V, and J datasets were separately interpolated in time by replacing each photometric observation by a weighted interpolation function. Several functional forms for these weights were examined, and the weighting function adopted was:

$$w_{i,j} = \frac{s^4}{s^4 + (t_j - t_i)^4} \tag{3.1}$$

where weight, $w_{i,j}$ at the point in time in question, t_j, is determined as compared to each other time t_i. The interpolated value, f_i, at $t = t_i$, where f can be any of the U, B, V, or J observed photometric values at time t_i, is then given by:

$$f_i = \sum_{j=1}^{N} w_{i,j}\ f_j \tag{3.2}$$

where N is the number of data points in the smoothing kernel.

This particular weighting function has one varying parameter, s, which indicates the time scale of the smoothing. Time differences $|t_j - t_i| < s$ are strongly smoothed, whereas $|t_j - t_i| > s$ are hardly smoothed. Each of the U, B, V, and J datasets were smoothed and interpolated by replacing each observed data point with this continuous basis function. After completion of smoothing and interpolation, a complete time series of U, B, V, and J photometry and radial velocity on a uniform time grid from 1990 to 2010 is available.

3.2 LOCHEST Interpolation

One drawback of the weighting function interpolation method is that continuity is not preserved as the function switches to a new set of data points in the kernel. For our analysis, however, differentiated quantities, such as angular diameter, were needed, and so a continuous first derivative was essential. Next, a variant of the widely used LOESS procedure (Cleveland et al., 1988), which we call LOCHEST: Local Cubic Hermite Estimate of Smoothing, was implemented. This is a two-step smoothing, interpolating procedure where:

1. Smoothing step: smoothed values and derivatives of the B, V, and J data were obtained at the original input points (in our case, observation times) using a variant of the LOESS procedure.

2. Interpolation step: the smoothed values were then interpolated to the final grid (here, a regular time grid) using a cubic hermite interpolation.

The LOESS step proceeds by replacing raw values of the photometric data with smoothed values obtained by fitting a low-order polynomial through nearby data points as a function of observation time. This step generates smooth function values and derivatives at each of the original epochs. Normally, the interpolating polynomial will vary with the selection of the data points included in the fit. This will give rise to discontinuities in the smoothed photometry when moving from one time interval $[t_{\rm i}, t_{\rm i+1}]$ to the next $[t_{\rm i+1}, t_{\rm i+2}]$. Therefore, a second-order polynomial least-squares fit was used to smooth the photometry at the observed epochs. This fit was weighted using the $w_{i,j}$ weighting function of §3.1.

The interpolation then proceeds by interpolating the smooth B, V, and J datasets to a uniform time grid using a cubic hermite interpolation. The Cubic hermite interpolating polynomial is uniquely determined by the function values and their slopes on each time interval $[t_{\rm i}, t_{\rm i+1}]$. This then ensures continuity of the function and first derivative across data interval boundaries. After completion of smoothing and interpolation, a complete time series of selected photometry is generated for a uniform time grid from 1990 to 2010 by increments of 0.01 years (figure 3.1). The radial velocity data were smoothed and interpolated in the same manner (figure 3.2). A source code for the interpolation method is included in appendix B.

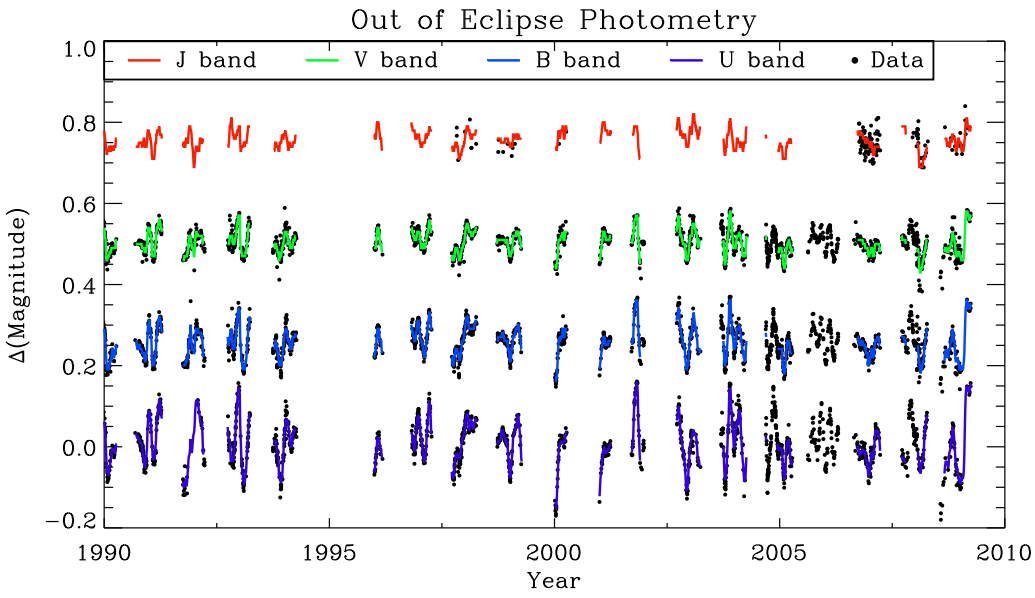

Figure 3.1: Interpolated out of eclipse photometry in U, B, V, and J bands.

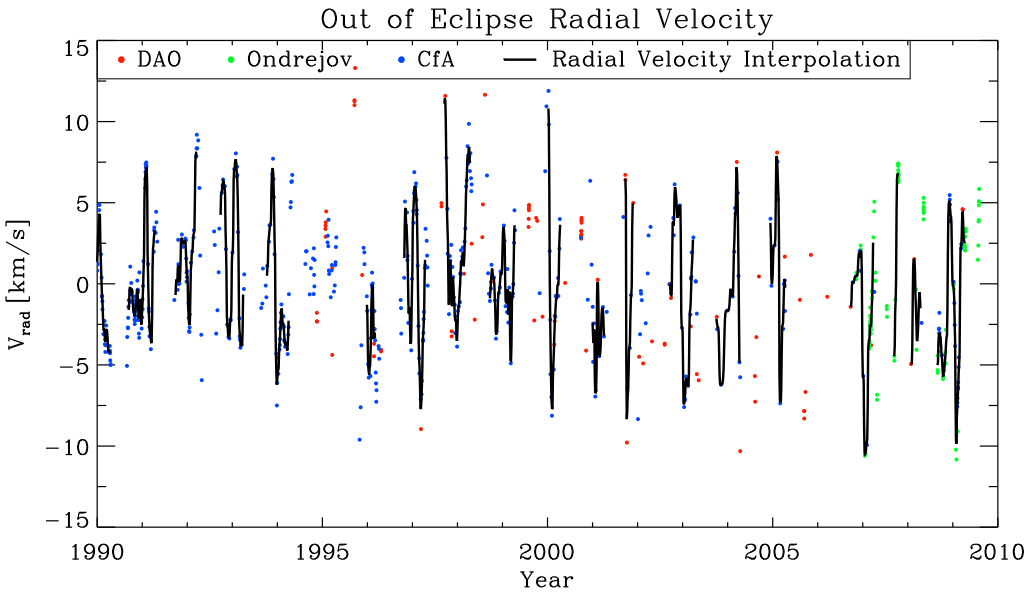

Figure 3.2: Interpolated radial velocity data.

Chapter 4

Deriving a Time Series of Stellar Parameters

The objective is to determine the best stellar model fit to the B, V, and synthetic J photometry at each point of the interpolated time series from 1990 to 2010. From each fit, we obtain the stellar effective temperature, T_{eff} and angular diameter, θ. The latter quantity is differentiated with respect to time and compared to the interpolated radial velocities. Unless the assumption that stellar pulsation drives both the photometric and radial velocity variability is incorrect, the mean slope between T_{eff} and $d\theta/dt$ then gives a Baade-Wesselink distance.

Synthetic photometry was derived by Bennett (2013) (private communication) from fitting the interpolated stellar fluxes from the models of Lejeune et al. (1997), using the bandpass response functions of Bessell et al. (1998). Model fluxes at the earth depend principally upon stellar effective temperature, angular diameter, and interstellar extinction. The extinction to ε Aur is significant with extinction in the visual wavelength, A_V, of 1.07 (Bennett, 2013).This must be corrected for prior to SED fits, and so the B, V, and J magnitudes were dereddened by $A_B = 1.40$, $A_V = 1.07$, $A_J = 0.302$ (Cox, 2000). It was found necessary to reject the U band dataset as means of the observers' photometry were internally inconsistent and discordant with archival U magnitudes from the SIMBAD database, lowering confidence in the avail-

able data. It is also notoriously difficult to generate accurate synthetic U photometry from model atmospheres, since the short wavelength cutoff of the U bandpass is defined by the atmosphere. For these reasons, U-band data were excluded from this analysis.

Model fluxes, f_λ, at the Earth were computed from the function

$$f_\lambda = \frac{1}{4}\ \theta^2\ F_\lambda(T_{eff})\ 10^{-0.4A_\lambda}, \tag{4.1}$$

where $F_\lambda(T_{eff})$ is the emergent model atmosphere (surface) flux for a star of effective temperature T_{eff}, θ is the stellar angular diameter, and A_λ is the extinction at wavelength λ, in magnitudes.

At each epoch, the dereddened, synthetic photometry was fit to the model grid of Lejeune et al. (1997) by Bennett (2013) using the SYNTH_MAG IDL photometric fitting package. The model grid was varied until the T_{eff} and θ produced an SED which matches the synthetic photometry (in a least squares sense). This procedure was carried out for ε Aur to derive T_{eff} and θ at each epoch of the regular time grid from 1990 to 2010.

The derived angular diameters were then numerically differentiated with respect to time to give $d\theta/dt$. If the intrinsic F star photometric and radial velocity, v_{rad}, variability originates from a common source, such as stellar pulsation in the fundamental mode, then $d\theta/dt$ and v_{rad} should be correlated. In practice, much of the interpolated photometric and radial velocity data were found to be largely uncorrelated. This was attributed to the incomplete sampling of one or both data sets over the period of

available data. Unfortunately, the best photometric coverage and the best radial velocity coverage tended to be at different times over the 1990-2010 period. However, the two year period of 1992-1994 was well-sampled in both datasets, as were selected times in the 2006-2009 period. The $d\theta/dt$ and v_{rad} data over these restricted periods were found to be slightly correlated (figure 5.2).

However, the Eaton (2013) dataset adequately samples the intrinsic radial velocity behaviour of the F star; it also overlaps times with improved photometric coverage. This radial velocity set, however, begins at mid-2008, and the ingress of eclipse begins about a year later. To make the photometry here useful, the stellar flux had to be corrected to that observed out of eclipse. By fitting and removing the low time-frequency onset of the eclipse while retaining the higher frequency intrinsic stellar variability. The fits used to correct for the early ingress stages of eclipse were piecewise linear and quadratic polynomials to the light curve. The radial velocity also showed a gradually increasing redshift in velocities due to the effects of eclipse. These were corrected for by smoothing the radial velocity with a 31-point boxcar (running mean) filter between the data of 2009.21 and 2010.75, and subtracting this low-frequency component. In this manner, both the B, V, and J photometry and radial velocity observations were approximately corrected for the onset of eclipse through the date of 2012.5.

Chapter 5

Deriving a Baade-Wesselink Distance

Both $d\theta/dt$ and v_{rad} provide independent determinations of (the physical phenomenon) stellar pulsation, but the key point is that one variable, $d\theta/dt$, measures the angular velocity of this pulsation, while the other variable, v_{rad}, measures actual stellar velocities. These are related by the distance to the star, so measuring the slope, m, of the regression line of v_{rad} against $d\theta/dt$ provides a direct measurement of the stellar distance. This is a variant of the Baade-Wesselink method commonly used to determine the distance to Cepheid variables.

5.1 Limb Darkening

The full amplitude of the stellar pulsation, v_{puls}, is not captured by the radial velocity, because of projection and limb darkening effects. These terms are commonly folded into the projection factor, p, where

$$p = \frac{v_{puls}}{v_{rad}}. \tag{5.1}$$

This factor must be determined in order to recover the distance. Although from Claret (2000), we obtain a p-factor of 1.42, the recent work of Neilson et al. (2012),

suggests a range of p values from 1.2 to 1.4. Neilson claims the Claret models do not accurately represent the extended atmospheres of supergiants. Therefore, we eventually intend to carry out a model atmosphere analysis to better estimate the relevant p-factor. For this work, we adopt a mean value of $p = 1.3$ (the midpoint of Neilson's range).

5.2 Distance Calculation

The general trigonometric distance determination is given by:

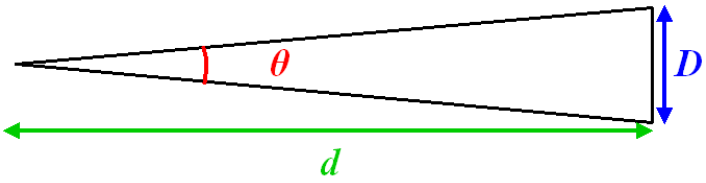

Figure 5.1: Trigonometric distance determination

$$D = \theta d \tag{5.2}$$

where θ is the angular diameter measured of the object, in milliarcseconds [mas], D is the linear diameter of the object, in astronomical units [AU], and d is the distance to the object, in kiloparsecs [kpc], as pictured in figure 5.1. The pulsational velocity, v_{puls}, is defined as the change in the linear size of the star over time, in units of [AU/yr].

$$v_{puls} = \frac{dD}{dt} = d\frac{d\theta}{dt} \tag{5.3}$$

In standard units,

$$1\frac{\text{AU}}{\text{yr}} = 4.7406\frac{\text{km}}{\text{s}} \tag{5.4}$$

The observed radial velocity, in our line of sight, is related to v_{puls} by the projection factor by:

$$v_{rad} = -\frac{v_{puls}}{p} \tag{5.5}$$

Substituting equation 5.3 into equation 5.5, we get:

$$v_{rad} = -\frac{d\frac{d\theta}{dt}}{p} \tag{5.6}$$

If we measure the slope of $v_{rad}/(d\theta/dt)$ then we can rearrange equation 5.6 to give:

$$d = -p\frac{v_{rad}}{d\theta/dt} \tag{5.7}$$

So well replace $v_{rad}/(d\theta/dt)$ as a general slope variable, m, and include the conversion factor, as described in equation 5.4. With p known, the distance d (in kpc) is given by the equation:

$$d = -\frac{mp}{4.7406} \tag{5.8}$$

5.2.1 Distance determination 1

The first distance determination was completed using the initially derived parameters. These parameters included the angular diameters as derived from model atmosphere fits of the B, V, and reconstructed J photometry from the relationships described in §2.4.1 (equation 2.2). The resulting correlation between the radial velocity data and the time derivative of angular diameters for this trial is pictured in figure 5.2. With

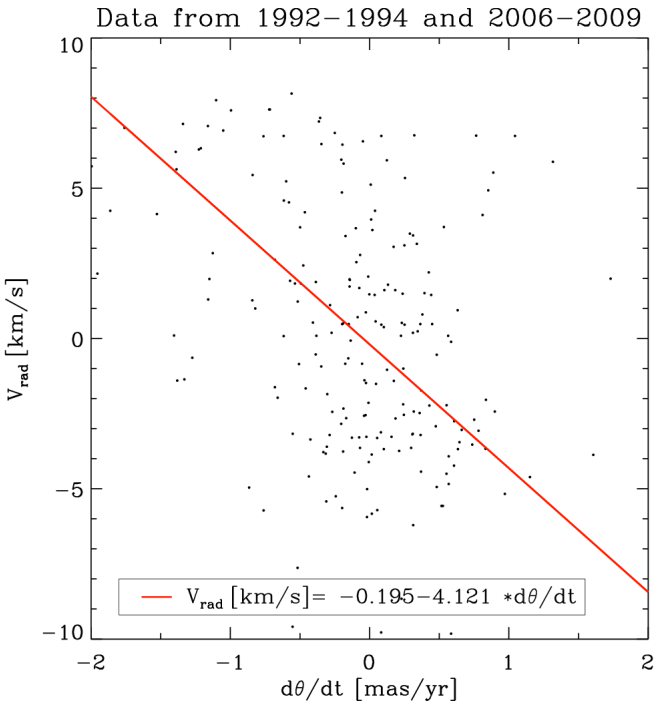

Figure 5.2: Relationship between radial velocity and changes in angular diameter used to derive a distance using infrared data reconstructed as described in §2.4.1.

the given slope, m, of :

$$m = -4.121 \frac{\text{km/s}}{\text{mas/yr}} \tag{5.9}$$

and p of 1.3, the estimated distance was found to be:

$$d \sim 1.13 \text{ kpc}. \tag{5.10}$$

5.2.2 Distance determination 2

Following the reconstruction of the J and H band data, from the relations inferred in §2.4.2, another distance estimate was attempted. As seen in figure 5.3, the slope is

now positive, with a value of

$$m = 4.011 \frac{\text{km/s}}{\text{mas/yr}}. \tag{5.11}$$

This results in a negative distance of

$$d \sim -1.10 \text{ kpc}, \tag{5.12}$$

which is an unphysical result. This positive correlation is a consequence of the method used to recreate the J and H band photometry from the relationships with V data (equation 2.3 and 2.4). Something appears to be either inconsistent with the data or in our analysis, and will be further discussed in §6

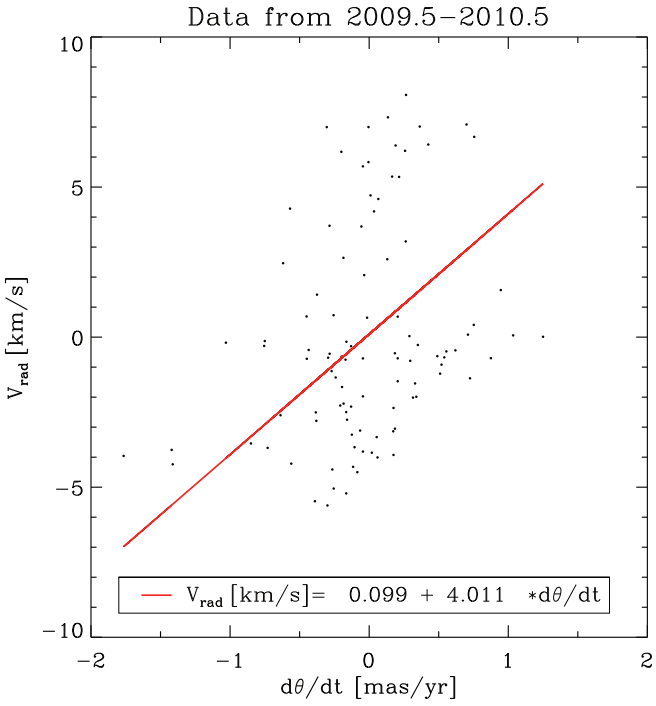

Figure 5.3: Relationship between radial velocity and changes in angular diameter used to derive a distance using infrared data reconstructed as described in §2.4.2.

5.2.3 Distance determination 3

Following a separate derivation of the J band data, (from equation 2.5), another distance estimate was attempted, using the J relation inferred in §2.4.3. As seen in figure 5.4, the angular diameters derived with these photometry vary in sync with radial velocity. Figure 5.5 also shows this correlation, for which we have an improved correlation coefficient of $R = -0.544$.

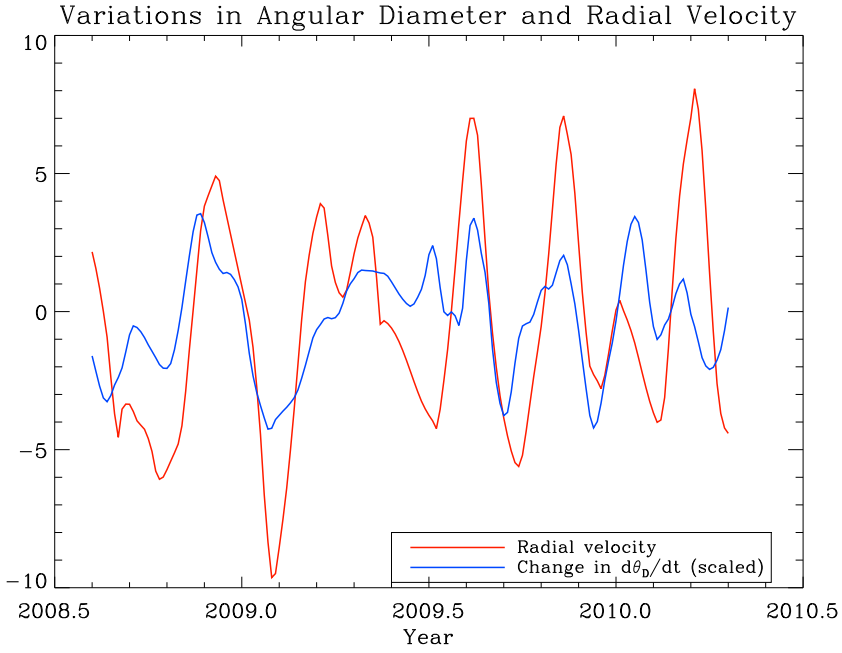

Figure 5.4: Correlation between radial velocity data and derived angular diameters near ingress of eclipse.

Using this information, the slope, m, was again calculated, with a result of :

$$m = -3.391 \frac{\text{km/s}}{\text{mas/yr}} \tag{5.13}$$

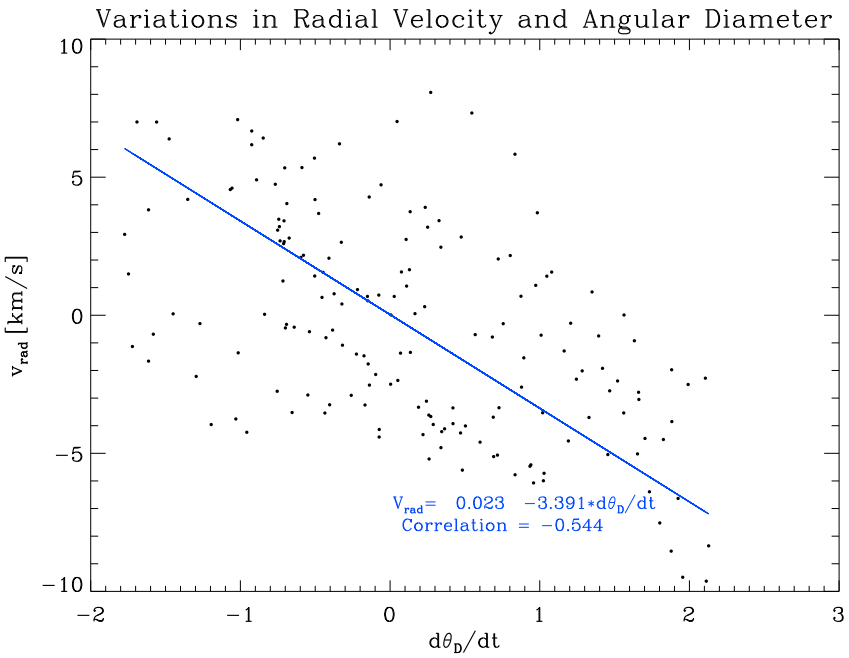

Figure 5.5: Relationship between radial velocity and changes in angular diameter used to derive a distance using infrared data reconstructed as described in §2.4.3.

as pictured in figure 5.4. For $p = 1.3$, the new estimated distance was found to be:

$$d \sim 0.93 \text{ kpc} \tag{5.14}$$

Chapter 6

Discussion

The values calculated in the previous section are all dependent on two factors: the angular diameters produced through the model atmosphere fits and the radial velocity data. The angular diameter values are in turn determined by the incorporated photometry. While the B and V data are both accurate and reasonably sampled in and out of eclipse, these values provide trustworthy information on the stellar pulsations of the F star. As discussed in §2.4, the IR data is too sparse to rpovide accurate results. Given this, we attempted to generate synthetic J-band photometry through colour-colour relations, as discussed in §2.4.1,2.4.2 and 2.4.3. These relationships, however, between the observed B, V, and J photometry appear more complex than anticipated, and the available IR photometry is too noisy and too limited in scope to allow us to accurately recover a realistic J-band time series spanning the 1990-2010 period. Stellar variability appears to be less than that at optical wavelengths (see figure 2.3); however, without a reliable IR data, it is not possible to adequately constrain model SED fits, and thus effective temperatures and angular diameters, at various epochs.

If the star is pulsating in the fundamental mode, we should see a strong correlation between the radial velocity data and the brightness of the star, but this behaviour is expected to be wavelength dependent. We can confirm that the observed variability

is consistent with fundamental mode radial pulsation of the F star. The observed brightness of the star at a particular wavelength depends on

1. the decreasing stellar diameter, and therefore the surface area, and

2. the increasing surface temperature.

The observed brightness at wavelength λ will vary as

$$f_\lambda \sim F_\lambda(T_{eff})\theta^2. \tag{6.1}$$

At short wavelengths, such as the B or V band passes, we expect the large temperature sensitivity of the stellar SED to overwhelm the modest increase in stellar emitting area. We also expect that further into the infrared, the opposite trend will prevail: here, the flux $F_\lambda \sim T_{eff}$, and changes in stellar surface area ($\sim \theta^2$) may dominate.

Infrared photometry compiled by Hopkins (2012) suggests that the sense by which the J band varies, ΔJ, is the same as ΔB and ΔV. Taranova & Shenavrin (2001) data suggests the opposite: ΔJ and ΔK vary oppositely of the ΔB and ΔV during pulsation. Without further observations, we cannot be certain of the correct behaviour of the IR SED, and thus cannot constrain T_{eff} and θ. We can, though, confirm that at short wavelengths, the variability of ΔV correlates positively with radial velocity, as seen in figures 6.1 and 6.2. This implies the star is brightest when smallest, confirming that T_{eff} variations dominate the B and V photometric variability.

While there is agreement between the derived distances in §5.2.1 and 5.2.3, this result is probably fortuitous. The error in these distance determinations are dominated

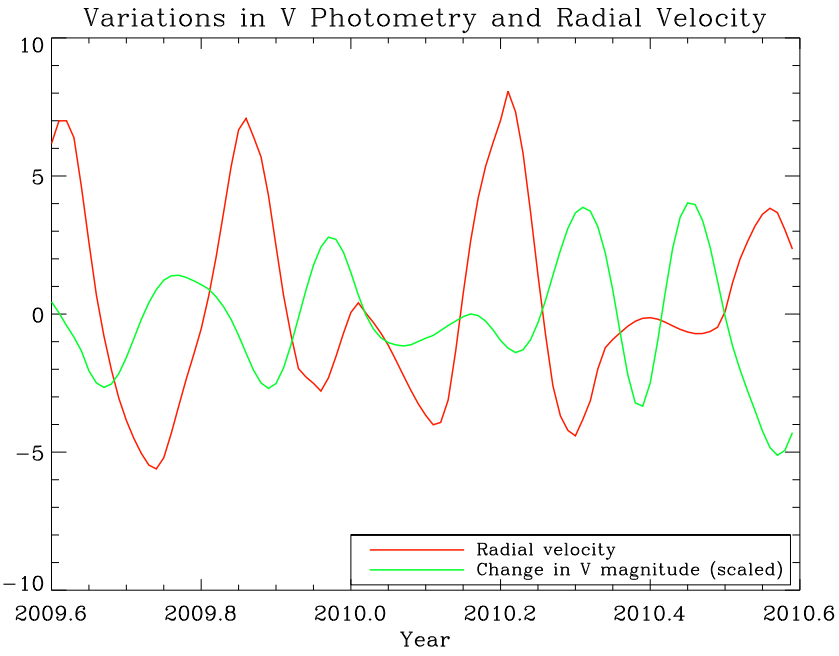

Figure 6.1: Radial velocity data and difference of the V band photometry from the mean. V band variations have been scaled for appearance.

by systematics, especially the uncertain colour-colour fits used to generate synthetic J photometry (as outlined in §2.4.1 and 2.4.3). Everything depends critically on these uncertain fits. The uncertainty in the distance estimate is large, and from this information, the distance is estimated between

$$600 < d < 1400\text{pc}. \tag{6.2}$$

The fact that there exists correlation between two measures (v_{rad} and $d\theta/dt$), derived from completely independent data sets, gives confidence to the method.

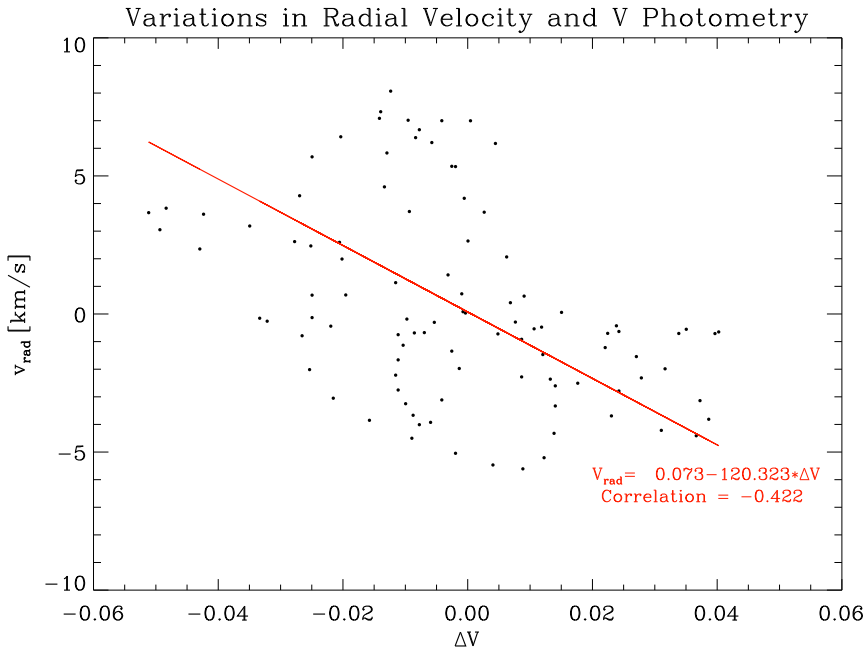

Figure 6.2: Correlation between radial velocity data and the difference of the V band photometry from the mean.

Chapter 7

Conclusions

We present here the first application of the Baade-Wesselink method to the irregularly pulsating star, ε Aur. The distance of 1.13 ± 0.21 kpc, found from our initial analysis (Wilson et al., 2012a,b) is not reliable, as the infrared observations are too limited and of too poor quality to accurately sample the stellar photometric variability at those wavelengths. We confirm that the star appears to be pulsating in the fundamental radial mode from the positive correlation between the variations in v magnitude and radial velocity. Therefore, in principle this analysis could provide a distance to the system, provided accurate data was available.

The observational sampling requirements of this approach are stringent, and the archival observations of ε Aur are not adequate for the task. Ideally, simultaneous photometric and radial velocity data would be collected over at least one observing season, outside of eclipse. Significant coverage in U, B, V, J, and K photometry, with concurrent radial velocity measurements over an observing season should provide enough data to complete a Baade-Wesselink distance determination and give accurate and meaningful results. Moreover, with a data set specifically acquired for this purpose, this technique would be established as another independent method of determining distances to many irregularly pulsating giant or supergiant stars.

Bibliography

Bennett, P. D. 2013, private communication

Bennett, P. D., & Wilson, C. K. 2013, in preparation

Bessell, M. S., Castelli, F., & Plez, B. 1998, A&A, 333, 231

Chadima, P., Harmanec, P., Yang, S., et al. 2010, Information Bulletin on Variable Stars, 5937, 1

Claret, A. 2000, A&A, 363, 1081

Cleveland, W. S., Devlin, S. J., & Grosse, E. 1988, Journal of Econometrics, 37, 87

Cox, A. N. 2000, Allen's Astrophysical Quantities, 4th edn. (New York: AIP Press)

Eaton, J. 2013, private communication

Guinan, E. F., Mayer, P., Harmanec, P., et al. 2012, A&A, 546, A123

Hopkins, J. L. 2012, `http://www.hposoft.com/campaign09.html`

Huang, S.-S. 1965, ApJ, 141, 976

Isobe, T., Feigelson, E. D., Akritas, M. G., & Babu, G. J. 1990, ApJ, 364, 104

Kloppenborg, B., Stencel, R., Monnier, J. D., et al. 2010, Nature, 464, 870

Kuiper, G. P., Struve, O., & Strömgren, B. 1937, ApJ, 86, 570

Lejeune, T., Cuisinier, F., & Buser, R. 1997, A&AS, 125, 229

Neilson, H. R., Nardetto, N., Ngeow, C.-C., Fouqué, P., & Storm, J. 2012, A&A, 541, A134

Stefanik, R. P., Torres, G., Lovegrove, J., et al. 2010, AJ, 139, 1254

Stencel, R. E. 2008, in Bulletin of the American Astronomical Society, Vol. 40, American Astronomical Society Meeting Abstracts #212, 207

Stencel, R. E. 2012, Journal of the American Association of Variable Star Observers (JAAVSO), 40, 618

Stothers, R. 1971, Nature, 229, 180

Taranova, O. G., & Shenavrin, V. I. 2001, Astronomy Letters, 27, 338

Turner, D. G. 2012, Journal of the American Association of Variable Star Observers (JAAVSO), 40, 502

van Leeuwen, F., ed. 2007, Astrophysics and Space Science Library, Vol. 350, Hipparcos, the New Reduction of the Raw Data

Wilson, C. K., Bennett, P. D., Hopkins, J. L., & McCandless, B. E. 2012a, `www.hposoft.com/Bennett/SpectroPoster.pdf`

—. 2012b, to appear in the Proceedings of the XIth Hvar Astrophysical Colloquium

Appendix A

IDL Code for Least-Squares Bisector Regression for 3 Variables

```
;_________________BEGIN_PROGRAM_3DBISECT_________________
;
pro 3dbisect, xin, yin, zin, as, bs, cs
;
;
; Written by : Christine K. Wilson, May 2012
;
; Purpose    : To calculate a least-squares bisector
;              planar fit to noisy, 3 dimensional data
;              using a generalization of the Isobe et al.
;              (1990) bisection method to 3 or more
;              variables.
; (See T. Isobe, E. D. Feigelson, M. G. Akritas, and
;      G. J. Babu. "Linear regression in astronomy." ApJ,
;      364:104  113 , November 1990. )
;
; Description: Fits a planar solution for the z variable,
;   of the form:
;                    z = as + bs*x + cs*y
;   from input data points [ xin[i], yin[i], zin[i] ].
;   Algorithm is further developed in comments.
;
; Input variables:
;      xin  : input of x variables
;      yin  : input of y variables (same length as xin)
;      zin  : input of z variables (same length as xin)
;
; Output variables:
;      as   : constant term of planar solution
;      bs   : x coefficient
;      cs   : y coefficient
;
;-------------------------------------------------------
;
;
; prepares a two dimensional arrays for xin with yin, yin
```

```
; with zin, and zin with zin.
;
    arrxy = [ transpose(xin), transpose(yin) ]
    arryz = [ transpose(yin), transpose(zin) ]
    arrxz = [ transpose(xin), transpose(zin) ]
;
; calculate an ordinary least squares (OLS) fit for each
; x, y, and z as a function of the other two variables.
; OLS(z|xy) : z = u1 + v1*x + w1*y
; OLS(x|yz) : x = u2 + v2*y + w2*z
; OLS(y|xz) : y = u3 + v3*x + w3*z
;
    OLSz = Regress( arrxy, zin, CONST=u1 )
    OLSx = Regress( arryz, xin, CONST=u2 )
    OLSy = Regress( arrxz, yin, CONST=u3 )
;
; prepare coefficients for standard form
; z = a1 + b1*x + c1*y , where b1=v1    , c1=w1
; z = a2 + b2*x + c2*y ,       b2=1/w2  , c2=-v2/w2
; z = a3 + b3*x + c3*y ,       b3=-v3/w3, c3=1/w3
; then calculate normal vectors to the z functions
; unit normal : ni = [bi,ci,-1]/Ti
;                    where Ti = sqrt(1+bi^2+ci^2)
;                    and i = 1, 2, or 3
; for fit 1:
;
    b1 = OLSz(0)
    c1 = OLSz(1)
    T1 = sqrt( 1 + b1^2 + c1^2 )
    n1 = [ b1 , c1 , -1 ] / T1
;
; for fit 2:
;
    v2 = OLSx(0)
    w2 = OLSx(1)
    b2 =   1 / w2
    c2 = -v2 / w2
    T2 = sqrt( 1 + b2^2 + c2^2 )
    n2 = [ b2 , c2 , -1 ] / T2
;
; for fit 3:
;
    v3 = OLSy(0)
    w3 = OLSy(1)
    b3 = -v3 / w3
```

```
    c3 =   1 / w3
    T3 = sqrt( 1 + b3^2 + c3^2 )
    n3 = [ b3 , c3 , -1 ] / T3
;
; produce D, product of Ti
;
    D = T1 * T2 * T3
;
; solution vector is ns = [bs, cs, -1] / D where bs and cs
; are given by:
;
    bs = ( b1*T2*T3 + b2*T1*T3 + b3*T1*T2 ) $
       / (   T2*T3  +   T1*T3  +   T1*T2  )
    cs = ( c1*T2*T3 + c2*T1*T3 + c3*T1*T2 ) $
       / (   T2*T3  +   T1*T3  +   T1*T2  )

    ns=[bs,cs,-1]/D
;
; Each OLS solution plane contains the centroid:
; [ <x>, <y>, <z> ], where <> denotes the mean value.
;
    zm=mean(z)
    xm=mean(x)
    ym=mean(y)
;
; Therefore, the constant term, as, is:
;
    as = zm - bs*xm - cs*ym
;
; return fit parameters to user
;
    return
    end
;------------------END_PROGRAM_3DBISECT--------------------
```

Appendix B

IDL Code for LOCHEST Interpolation

```
;_________________BEGIN_PROGRAM_LOCHEST_____________________
pro LOCHEST, xin, yin, s, xout, yout
;
;
; Written by : Christine K. Wilson, July 2012
;
; Purpose    : To complete a smoothing and cubic hermite
; interpolation of noisy data.
;
; Description: This algorithm was developed to complete a
;              LOCHEST interpolation, where LOCHEST :LOcal
;              Cubic Hermite Estimate of SmooThing.
;              Following a similar concept as the LOWESS
;              (LOcally WEighted Scatterplot Smoother),
;              the LOCHEST method is a two step
;              interpolator:
;   1. The input y values are smoothed at the original
;      input x values, using a weighted quadratic of the
;      form:
;             w_i,j =  s^4 / ( s^4 + (x_j - x_i)^4 )
;      where s is the smoothing parameter. For a given
;      x_j, |x_j - x_i| < s are strongly weighted, and
;                       > s are weakly weighted.
;   2. The smoothed y values are then interpolated using a
;      cubic hermite interpolator to ensure continuity in
;      the first derivative.
;
;
; Input variables:
;      xin  : input of independent variables
;      yin  : input of dependent variables (same length as
;             xin)
;      s    : smoothing parameter
;
; Output variables:
;      xout : output of
```

```
;      yout : output of interpolated y values, computed
;             using a cubic hermite interpolation.
;
; Externals:
;      hermite : function from IDL library
;
;-------------------------------------------------------
;
;----------------------SMOOTHING STEP-----------------------
;
; determine number of elements in xin and yin
;
    nxin = n_elements( xin )
    nyin = n_elements( yin )
;
; create array, of the same dimension as xin, for weights
;        array, of 3 dims, for quadratic fit coefficients
;        array, of the same dimension as xin, for smoothed
;               y values
;
    wt      = dblarr( nxin )
    ysm     = dblarr( 3 )
    ysmooth = dblarr( nxin )
;
; calculate all weights by looping over all xj for each xi
;
    for i=0, nxin-1 do begin
      for j=0, nyin-1 do begin
        wt[j] = ( s^4 ) / ( s^4 + ( ( xin[j]-xin[i] )^4) )
;
; prepare conditions for endpoints
;
        if i eq 0 then begin
          jmin = 0
          jmax = 2
        endif else if i eq nyin-1 then  begin
          jmin = nyin-3
          jmax = nyin-1
        endif else begin
;
; prepare conditions for neighbouring points
;
          jmin = i-1
          jmax =i+1
        endelse
```

```
;
; set weights for all above cases equal to 1
;
        wt[jmin:jmax] = 1.0d0
      endfor
;
; complete a quadratic fit for each point xi with weights
; for a new smoothed y
;
      ysm = POLYFITW( xin, yin, wt, 2, /double )
;
; produce new smoothed y values from the quadratic
; coefficients
;
      ysmooth[i]= poly( xin(i),ysm )
    endfor
;
;--------------------INTERPOLATION STEP-------------------
;
; find minimum and maximum x values, and produce a regular
; x grid, xout, for which each x is seperated by dx.
;
    xmin   = min(xin)
    xmax   = max(xin)
    dx     = 0.01
    xrange = (xmax-xmin)/dx
    nxout  = dindgen(xrange)
    xout   = xmin + nxout*dx
    nxout  = n_elements(xout)
    yout   = dblarr(xout)
;
; send smoothed y values for each xin into the cubic
; hermite interpolator, 'hermite', (available in the IDL
; library) to produce interpolated y value, yout, at each
; xout.
;
    yout=hermite(xin,ysmooth,xout)
;
; return interpolated values to user
;
    return
    end
;
;------------------END_PROGRAM_LOCHEST--------------------
```